Journal of The Electrochemical Society

Electrochemical Behavior of Electrolytic Manganese Dioxide in Aqueous KOH and LiOH Solutions: A Comparative Study

Electrochemical Behavior of Electrolytic Manganese Dioxide in Aqueous KOH and LiOH Solutions: A Comparative Study

Eric D. Rus,[a] Geon Dae Moon,[a] Jianming Bai,[b] Daniel A. Steingart,[c] and Can K. Erdonmez[a,*,z]

[a]*Sustainable Energy Technologies Department, Brookhaven National Laboratory, Upton, New York 11973, USA*
[b]*National Synchrotron Light Source II, Brookhaven National Laboratory, Upton, New York 11973, USA*
[c]*Mechanical and Aerospace Engineering and the Andlinger Center for Energy and the Environment, Princeton University, Princeton, New Jersey 08540, USA*

As an inexpensive and high capacity oxidant, electrolytic manganese dioxide (γ-MnO_2) is of interest as a cathode for secondary aqueous batteries. Electrochemical behavior of γ-MnO_2 was characterized in aqueous 5.0 M KOH and LiOH solutions, and found to depend strongly upon cation identity. In LiOH and mixed LiOH / KOH solutions, Li-ion intercalation appeared to operate in competition with proton intercalation, being favored at higher [Li^+] and, for mixed electrolytes, lower sweep rates. Electrochemical and in situ X-ray diffraction data indicated that γ-MnO_2 underwent a chemically irreversible transformation upon the first reduction in LiOH solution, while in KOH solution, structure was largely unchanged after the first cycle. These experiments with γ-MnO_2 as well as with a closely-related, ramsdellite-like sample, suggest that depending on sample morphology/rate capability, the irreversible process proceeds either through a solid-solution reaction or a two-phase reaction followed by a solid-solution reaction. While discharge capacity and capacity retention during galvanostatic cycling of γ-MnO_2 were worse in LiOH than in KOH solution, some improvement was noted in a mixed LiOH/KOH solution.

Manuscript submitted August 10, 2015; revised manuscript received November 24, 2015. Published December 9, 2015.

Electrolytic manganese dioxide (EMD or ε/γ-MnO_2) is the material most commonly employed as the cathode in primary alkaline batteries and primary non-aqueous lithium cells owing to its relatively low cost, low toxicity, high reduction potential, and high gravimetric capacity. Unfortunately, MnO_2-based secondary cells tend to have limited cycle life, due to the conversion of active material into electrochemically inactive or electronically resistive phases, such as hausmannite (Mn_3O_4) or hetaerolyte ($ZnMn_2O_4$) in aqueous cells,[1,2] and to pulverization associated with large changes in volume with state of charge.[3] Under certain conditions, however, γ-MnO_2 can be cycled with relatively good capacity retention. Major criteria for reversible cycling are to limit the depth of discharge to minimize the solubility of manganese in lower oxidation states, and to avoid the formation of soluble high oxidation state species during charging (i.e. MnO_4^{2-}).[4,5,6,7] It has also been reported that the use of LiOH instead of KOH as the electrolyte can improve the cycle life of γ-MnO_2.[8]

The structure of γ-MnO_2 is highly defective both in terms of type and concentration of defects. According to the De Wolff model, the structure is thought to be an intergrowth of ramsdellite and pyrolusite layers (Fig. 1).[9,10] Both phases have tunnel-structures, as is apparent from the viewpoint in Fig. 1. γ-MnO_2 also contains microtwinning defects, which introduce kinks to the tunnel structure.[10] Manganese vacancies can also be present and necessitate the incorporation of protons (Ruetschi protons) in the structure to maintain charge balance.[12]

In aqueous KOH or NH_4Cl media (in the case of a Leclanché cell), the reduction of the Mn^{4+} to Mn^{3+} is accompanied by the incorporation of protons into the tunnels in the structure (along the *b* direction as shown in Fig. 1) to maintain charge balance.[2] In non-aqueous Li-ion containing media, lithium ions are incorporated into the material instead. Most published work in Li-ion containing media has considered heat-treated forms of γ-MnO_2. Heat treatment, even at relatively mild temperatures, can significantly affect the electrochemical behavior of the material in both KOH solutions[13] and non-aqueous Li-ion media.[14] This complicates direct comparison of published data for proton and Li-ion insertion. Jouanneau et al. did make a comparative study of numerous MnO_2 samples with a range of defect contents in aqueous KOH solutions and non-aqueous LiOH solutions, with only a mild heat-treatment.[15] Minakshi et al. compared MnO_2 in KOH and LiOH solutions, but only in the presence of zincate ($Zn(OH)_4^{2-}$), which can affect the behavior of the material by reacting with the reduced form.[16]

In light of reports of improved capacity retention in LiOH solutions (in comparison to KOH solutions), and in the interest of comparing proton and lithium ion uptake by non-heat treated material, we carried out a comparative study of γ-MnO_2 in aqueous LiOH and KOH solutions. In situ X-ray diffraction measurements were used to elucidate the structural changes associated with the electrochemical behavior. Ramsdellite-like MnO_2 (R-MnO_2) was also investigated as a less-defective reference material, which is more readily characterized via diffraction, in order to clarify transformation mechanisms in γ-MnO_2.

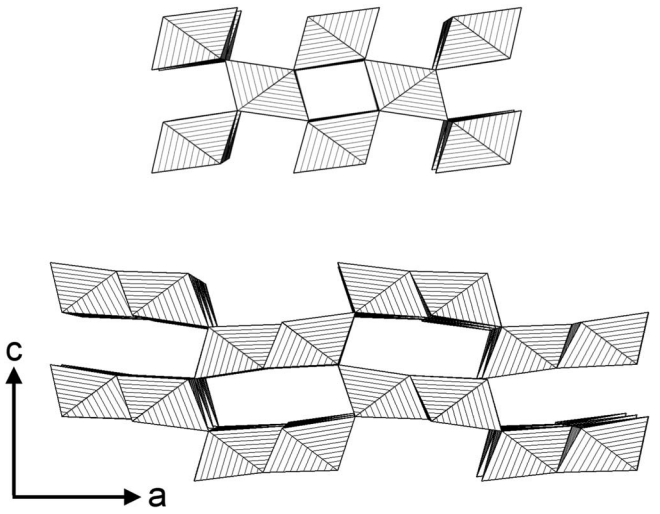

Figure 1. Representation of (a) pyrolusite and (b) ramsdellite structures as [MnO_6] octahedra, with the a and c-directions of ramsdellite indicated. These diagrams were constructed using reported parameters.[11,19] To provide a sense of scale, the Mn-O bond length is about 1.89 Å, implying an octahedral edge length ~2.7 Å for idealized octahedral geometry.

*Electrochemical Society Active Member.
[z]E-mail: erdonmez@gmail.com

Experimental

Electrochemical measurements.— Electrochemical measurements were carried out in a three electrode configuration, using a BioLogic VSP-300, an Arbin BT2000, or a Metrohm μAutolab III. Electrolytes were prepared with 18 MΩ cm^{-1} water (prepared with Millipore Direct-Q 3 UV), puriss grade KOH, or reagent grade $LiOH \cdot H_2O$, both from Aldrich. The solubility of LiOH in water at room temperature is 5.1 – 5.2 M.[17] Therefore, the 5.0 M LiOH solutions were close to saturation and electrolyte preparation required heating the solution at 100°C and cooling back to room temperature.

Working electrodes were prepared by mixing γ-MnO_2 (electrolytic manganese dioxide, Tronox), graphite (Timcal C-NERGY C45), carbon black (Timcal Super P Li), and PTFE suspension (Sigma Aldrich, diluted to a 6% wt suspension in water) in a 62:16:16:5 dry weight ratio. The dry components were mixed together first. The PTFE suspension and some additional water were then added. This mixture formed a coherent mass which was rolled flat on a glass microscope slide to form a sheet approximately 0.25 mm thick. The mixture of carbon black and graphite was chosen because preliminary studies showed improvement in active material utilization and apparent oxidation kinetics in LiOH solutions when using high surface area carbon. Such electrodes were mechanically fragile, however, and the addition of graphite to the mixture was necessary to make more robust electrodes.

$Ni(OH)_2$/NiOOH counter and pseudoreference electrodes were prepared by mixing NiOOH (Kansai Catalyst Company), graphite and PTFE suspension in a 50:45:5 dry weight ratio. The counter electrodes were electrochemically reduced to $Ni(OH)_2$ in separate cells prior to measurements with γ-MnO_2.

Expanded Ni mesh (0.1 mm thick, with 1.1 × 2.5 mm openings, from Dexmet Corp.) served as the current collector for both the working and counter electrodes. Pieces of the active material/carbon/PTFE sheet were cut out and pressed on either side of the current collector. They were then placed in a folded piece of aluminum foil and pressed between two 2-inch diameter platens on a uniaxial Carver press at 3000 pounds for 1 minute. The electrode was not confined on the sides during compression, allowing the area to increase slightly. Strips of nickel foil were crimped to the electrodes for electrical contact.

The working electrode active mass used in these measurements was ∼8 mg for cyclic voltammetry measurements and ∼12 mg for galvanostatic measurements. Extra care was taken in keeping the active mass consistent for the measurements in LiOH – KOH mixtures with low LiOH content. In these cases, the total amount of dissolved Li^+ in the cell could in principle change significantly during measurements by incorporation into the electrode, so it was desirable to keep variation in the bulk solution Li^+ concentration consistent between measurements.

For benchtop measurements, borosilicate glass shell vials served as the cell container. No stack pressure was applied to the electrodes. The electrochemical cell used for in situ synchrotron measurements employed transmission geometry, with the beam passing through a hole in the counter electrode prior to reaching the working electrode. The cell body was laser cut from acrylic sheets, and an approximately 0.5 to 1 mm layer of acrylic formed the window on the side of the cell through which the beam entered. A 75 μm PEEK (polyether ether ketone) film formed the window on the exit side of the cell. Silicone elastomer gaskets were used to seal the cell against solution leakage. A diagram of the cell used for in situ measurements is included in the supporting information (Fig. S1).

Potentials are referred to the reversible hydrogen electrode (RHE). Either a Hg/HgO reference or a $Ni(OH)_2$/NiOOH pseudoreference electrode was used. In each case, the reference electrode was filled with a solution of the same composition as was used in the working and counter electrode compartment, and was calibrated against a RHE in the same solution. The $Ni(OH)_2$/NiOOH pseudoreference electrodes were allowed several days to equilibrate in solution prior to starting measurement, particularly in the case of LiOH containing solutions, which took longer to settle. The potential of the $Ni(OH)_2$/NiOOH electrodes was stable on the timescale needed for the measurements in this work (see supporting information fig. S2). The potential of the Hg/HgO electrodes was +0.930 V vs RHE, which is in good agreement with the reported value of 0.9256 V.[18] As a point of reference, the $Zn/Zn(OH)_4^{2-}$ (0.25 M) potential in 5 M KOH is about −0.45 V vs RHE.[19]

To facilitate comparison of data in the present work with published electrochemical data in Li-ion containing organic media, potentials are referred to Li/Li^+ at some points. The conversion from the RHE scale was made by:

$$E_{Li/Li^+} = E_{RHE} - 2.303\frac{RT}{F}pH - \left(E^0_{Li/Li^+} + \frac{RT}{F}\ln[Li^+]\right) \quad [1]$$

where $E^0_{Li/Li^+} = -3.04$ V vs NHE and E_{RHE} is the potential referenced to the RHE. The pH of the 5.0 M LiOH solution was taken to be 14.36,[20] and the pH of the 0.05 M LiOH + 4.95 M KOH solution was taken to be 14.7. A potential of 0 V vs RHE would be +2.16 V vs Li/Li^+ (5 M) and +2.26 V vs Li/Li^+ (0.05 M).

Galvanostatic cycling was carried out at 20 mA/g for both oxidation and reduction. This would correspond to a rate of C/15.4, assuming a theoretical one-electron capacity of 308 mAh/g, though the true capacity would be lower due to cation vacancies and Mn^{3+} initially present in the electrode. A +1.35 V vs RHE constant potential step with a 2 mA/g or 10 hour cutoff was included after the galvanostatic oxidation step. A 1 hour open circuit period was included after the oxidation and reduction periods.

X-ray measurements.— Diffraction patterns of γ- and R-MnO_2 powders were collected using a Rigaku SmartLab diffractometer using Cu K_α x-rays (1.54059 Å). In situ diffraction measurements were carried out at the X14A beam line at the National Synchrotron Light Source (NSLS) at Brookhaven National Laboratory. The X-ray wavelength was tuned to and fixed at 0.780138 Å at X14A with a sagittal focusing monochromator, and a linear detector mounted at about 1400 mm away from the sample position was used to take the XRD patterns. To facilitate comparison of data sets with differing wavelengths, the diffraction patterns are shown in terms of Q, the magnitude of the scattering vector:

$$Q = \frac{4\pi}{\lambda}\sin(\theta) \quad [2]$$

Results and Discussion

Diffraction patterns of γ-MnO_2 and R-MnO_2.— The diffraction pattern of the γ-MnO_2 used in the present work shows a relatively small number of broad peaks, suggesting a highly defective structure (Fig. 2a). The indices in the figure are written according to the orthorhombic Pnma space group (no. 62),[21] though other authors have used different settings of this group. Because the (212)/(402) doublet and the (020)/(610) peaks of the ideal ramsdellite structure are completely merged in the γ-MnO_2 pattern, and because the barely discernible (301) line has almost merged with the (210) line, we classified this sample as having a type III pattern, according to the classification scheme of Chabre and Pannetier. This is consistent with EMD deposited at high current density.[10] This pattern is of the class that would index well with a hexagonal structure if not for the broad peak at low Q,[10] and the pseudo-hexagonal indexing has been indicated in the figure as $(hkl)_h$. Since the merging of peaks complicates determination lattice parameters for an orthorhombic cell, values calculated for a pseudo-hexagonal cell are given in Table I.

Ramsdellite-like MnO_2 (R-MnO_2) was synthesized by heating $LiMn_2O_4$ (Aldrich) in aqueous 2.5 M H_2SO_4 solution for 24 hours at 95°C,[22,23,24] and the product was separated from solution by centrifugation and rinsed with water. An unidentified crystalline impurity was present in the initial product, but could be removed by washing with alkaline aqueous solution. The diffraction pattern of the purified R-MnO_2 (Fig. 2b) is in agreement with that reported in previous

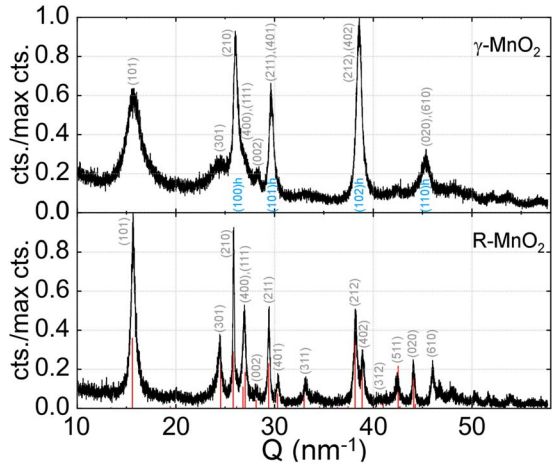

Figure 2. X-ray diffraction patterns of γ-MnO_2 and ramsdellite-like MnO_2 with overlay of peak assignments and data (in red) from Thackeray et al.[17] Peak indices (assuming an orthorhombic unit cell) are shown above the diffraction patterns. Additionally, pseudo-hexagonal indices are shown in blue below the γ-MnO_2 pattern. (Cu K_α, $\lambda = 1.54059$ Å).

work.[23,24] The (210), (211), (212), and (402) peaks were used in calculating the lattice parameters for the R-MnO_2 since these are expected to be unaffected by De Wolff disorder.[10]

The γ- and R-MnO_2 were characterized (Table I) in terms of degree of microtwinning (Tw) and level of De Wolff disorder (P_r, the pyrolusite fraction) using the method of Chabre and Pannetier, which is based upon simulated diffraction patterns for model structures.[10] A brief description of the calculation is given in the supporting information. For γ-MnO_2, the merging of the doublets prevents calculation of Tw, but indicates this sample has extensive (Tw>70%) microtwinning. The Tw and P_r values obtained for R-MnO_2 (Table I) are in good agreement with those reported by Chabre and Pannetier for a sample obtained from M.M. Thackeray.[10]

There is a close correspondence between the diffraction patterns of γ-MnO_2 and R-MnO_2 which is a consequence of the common local structural motifs shared by the two phases. The most important distinction between the patterns is that some sets of neighboring peaks which are distinct in the pattern of R-MnO_2 are present as merged, broad single peaks in the case of γ-MnO_2. The full explanation for this difference requires detailed modeling of the defect structure in γ-MnO_2,[10] but it is important to note that this is simply a consequence of lack of long-range order in γ-MnO_2 and that the data is consistent with essentially identical short-range (e.g. < 1.0 nm) bonding between the two materials. (We have verified this correspondence using pair distribution function analysis which we plan to report elsewhere).

Electrochemical behavior.— The electrochemical behavior of γ-MnO_2 in KOH, LiOH and mixed LiOH/KOH solutions was characterized using potentiostatic (Fig. 3) and galvanostatic methods (Fig. 4). Cyclic voltammograms at different potential sweep rates are shown in Fig. 3, with the currents normalized to active mass and to sweep rate. The voltammograms in KOH solution are in good agreement with those previously reported,[10] showing two to three reduction processes (here denoted R1 to R3) over the +1.35 V to +0.6 V range. Process R1 has previously been attributed to reduction of surface sites (or sites near manganese vacancies),[25,26] and R2 and R3 to reduction of ramsdellite domains and pyrolusite domains, respectively.[10,27] These same processes were also evident in the potential profiles observed during galvanostatic cycling (Fig. 4). An additional reduction process was observed in the galvanostatic data at about +0.52 V since a wider potential window was used in that measurement. This process corresponds to the formation of $Mn(OH)_2$ (pyrochroite) via a mechanism involving dissolved Mn^{3+} species.[6,28,29] Upon subsequent galvanostatic oxidation, $Mn(OH)_2$ was reoxidized to form birnessite, corresponding to the plateau at about +0.65 V. Differential capacity curves for the first and second cycles are shown at the right in Fig. 4. In KOH solution, the differential capacity profile agrees well with the cyclic voltammogram collected at the slowest sweep rate.

Plots of $\partial\log|i_p|/\partial\log|v|$, where i_p is the peak current and v is the scan rate, gave slopes of 0.86 and 0.82 for reduction processes R1 and R2, and 0.70 for oxidation process O2 (see supporting information Fig. S5). For a process under kinetic control, i_p would be directly proportional to v, while a diffusion controlled process would have i_p

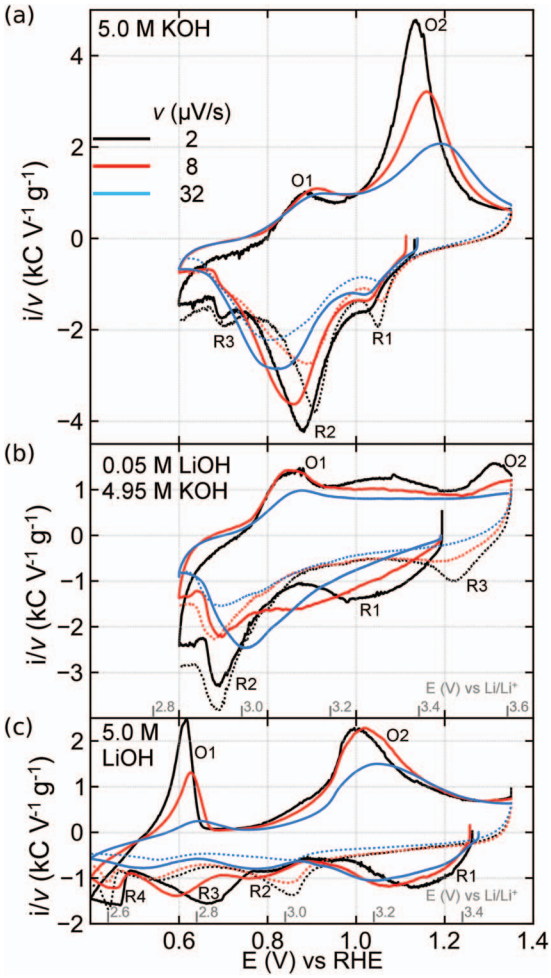

Figure 3. Cyclic voltammograms of γ-MnO_2 at 2, 8, and 32 μV/s in (a) 5.0 M KOH, (b) 0.05 M LiOH + 4.95 M KOH, and (c) 5.0 M LiOH solutions. The current was normalized to both the active mass and scan rate (v). The first cycle is shown as a solid trace, and the second cycle negative-going sweep is shown as a dotted line. In (b) and (c), the calculated potential vs Li/Li^+ is noted. Reduction and oxidation peaks are labeled R* and O* to clarify the discussion.

Table I. Microtwinning (Tw) and De Wolff disorder (P_r) parameters of γ- and R-MnO_2, determined from diffraction data using the method of Chabre and Pannetier.[10] The pseudo-hexagonal lattice parameters for γ-MnO_2 were calculated based on the $(100)_h$ and $(101)_h$ peaks, while those for R-MnO_2 were based on the (210), (211), (212), and (402) peaks, the positions of which should not be strongly affected by disorder. Calculation details are given in supporting information.

Sample	Tw	P_r	lattice parameters (Å)		
γ-MnO_2	>70%	0.40	2.79	4.44	
R-MnO_2	24%	0.26	*a*: 9.36	*b*: 2.84	*c*: 4.45

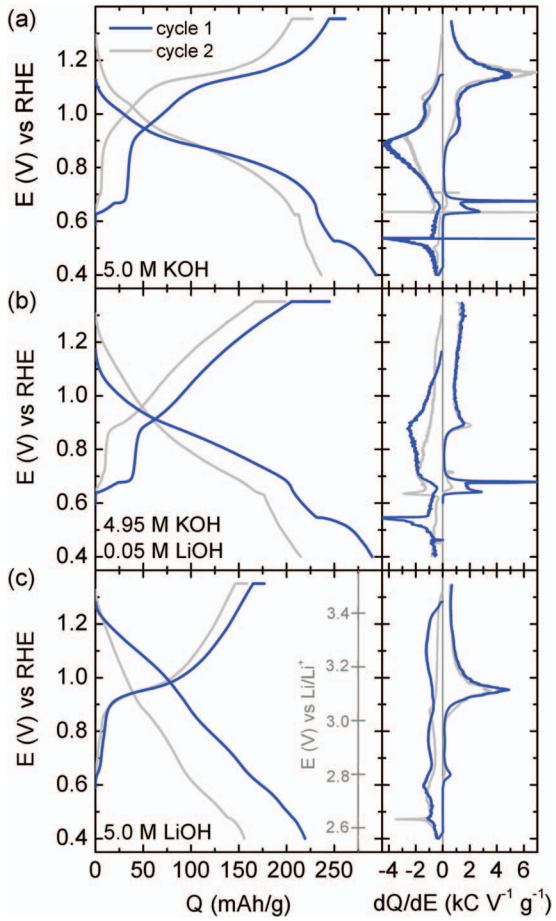

Figure 4. Galvanostatic reduction / oxidation profiles of γ-MnO_2 in (a) 5.0 M KOH, (b) 0.05 M LiOH + 4.95 M KOH and (c) 5.0 M LiOH solutions at 20 mA/g, with a constant potential hold at +1.35 V vs RHE (2 mA/g or 10 h cutoff) after the galvanostatic oxidation. The first and second cycles are shown. The calculated potential vs Li/Li^+ is noted in (c). In each case, differential capacity curves are shown at the right.

proportional to $v^{1/2}$. This suggests that the reduction processes are kinetically limited, while the oxidation process may have some diffusion constraints.

The behavior of γ-MnO_2 in Li^+-containing solutions differed drastically from that observed in KOH solution. Reduction commenced at a potential over 100 mV more positive in 5.0 M LiOH solution, and showed three to four peaks (denoted R1 to R4) in the first negative-going sweep, depending on the potential sweep rate, and two oxidation peaks in the positive-going sweep. A wider potential window was used in LiOH solution since process R3 shifted drastically with sweep rate, and would have been outside the more restricted window at higher sweep rates. In the context of aqueous Li-ion cells, several transition metal oxides have been found to have similar Li-ion intercalation behavior in both aqueous and non-aqueous media.[30] It is not clear how close a comparison can be drawn between results of the present study and published results for γ-MnO_2 in non-aqueous Li^+-containing solutions, since the material used in the latter setting was typically heat treated. Mildly heat-treated EMD was reported to show two processes at about +3.3 V and +2.8 V vs Li/Li^+ during the first reduction in organic media.[14,31,32]

The fact that up to four reduction processes were observed in the first negative-going sweep in the present work, while only two are reported for reduction in organic media, suggests that protons from water are involved in at least two of the processes. The peak position for the first reduction process R1 at about +1.14 V vs RHE (Fig. 3c, referring to the 2 μV/s voltammogram) approximately corresponds to that reported in organic media. The relative charge associated with reductions R2 and R3 depended strongly upon sweep rate. As the potential sweep rate was increased, the process R3 became less prominent and shifted to more negative potentials. The process R2 was less drastically affected by sweep rate in terms of peak position and scan rate-normalized peak current. Comparison with literature data regarding γ-MnO_2 reduction in organic electrolytes suggests that peak R2 corresponds to Li-ion insertion; reduction R3 is likely specific to water-based electrolytes, representing e.g. proton insertion.

The first reduction process R1 in LiOH solution was chemically irreversible, while process R1 in KOH solution was chemically reversible. Reversal of the sweep direction immediately after completion of the first reduction process in LiOH solution confirmed that the irreversibility of this process was *not* connected to any lower potential processes (Fig. S6). The charge associated with the first reduction process in LiOH (92 mAh/g) was somewhat higher than that for first reduction process in KOH (55 mAh/g). The differences in charge and reversibility indicate that the first reduction processes in KOH and LiOH solutions are not analogous, or that an additional process(es) contributed to the charge passed in the LiOH solution. Peaks R2 and R3 were observed in subsequent cycles in LiOH solution, though with slightly different positions.

The final reduction process R4 in the negative-going sweep in LiOH corresponded to the formation of $Mn(OH)_2$. Comparing Fig. 4a and 4c, this process is less prominent in LiOH solution than in KOH solution. This is possibly due to differing solubility of Mn^{3+} in the two solutions. It has been found that significant ion pairing may occur in LiOH, while it was not noted in KOH solutions.[33] This means that fewer hydroxide ions would be available to complex with Mn^{3+} in LiOH solution, which would decrease its solubility.

Oxidation process O1 in the positive-going sweep (Fig. 3c) corresponds to $Mn(OH)_2$ oxidation, as it does in KOH solutions. Two processes are generally reported for the oxidation of manganese dioxides in Li-ion-containing organic media, whereas only one is observed here at +1.0 V (disregarding the $Mn(OH)_2$ oxidation peak). The potential range used here was too narrow to include the more positive of the two oxidation processes observed in organic media, which is typically at about +3.4 V to +3.5 vs Li/Li^+.[32] This higher potential oxidation process was observable when a less alkaline LiOH + Li_2SO_4 solution was used (Fig. S7). (At lower pH, the onset of oxygen evolution is shifted to more positive potentials relative to Li/Li^+.)

The voltammetric profile and galvanostatic discharge profiles observed in the present work are markedly different from those reported by Minakshi et al. in 5.0 M or saturated LiOH solutions.[8,16,34] In that work, only a single reduction process, or two closely spaced reduction processes, spanning the potential range from about +1.4 to 1.1 V vs RHE were evident (assuming negligible polarization of the Zn anode used in that work). The difference between the published work and that reported here could be due to a difference in the form of manganese dioxide used; the material used in the earlier work displayed a different diffraction pattern than the one we observed here.[16] Electrochemical data for MnO_2 in KOH solutions were also reported in that work, with a voltammetric profile differing significantly from that observed here, also suggesting that the material used in the earlier work might be different from that used here.

In the mixed KOH/LiOH electrolyte, the reduction profile of the γ-MnO_2 resembled that in 5.0 M LiOH solution at slower scan rates and that in 5.0 M KOH solution at higher scan rates. The transition between the two behaviors occurred at about 8 μV/s. In mixed electrolytes with a higher fraction of LiOH, the voltammetric profile resembled in that in solution with LiOH alone at all sweep rates. Even though the total amount of Li^+ in the cell (corresponding to 5.4 mAh) was more than adequate to compensate the charge passed during reduction of the γ-MnO_2 electrode (~1.5 mAh cyclic voltammetry, ~3 mAh galvanostatic cycling measurements), it seems possible that mixed or competitive uptake of protons and lithium ions takes place. It has been noted that competitive uptake is to be expected in dilute Li^+ aqueous solutions.[35]

For the experiments using the mixed electrolyte, there were one to three oxidation peaks in the positive-going sweep, depending on the sweep rate. The more prominent of these have been labeled O1 and O2 in Fig. 3b. The potential range between them was relatively flat and the current scaled almost proportionally with scan rate in a manner resembling that of a capacitor. It is not entirely clear why such behavior should arise in the positive-going sweep only, while the negative-going sweep shows a more battery-like profile with well-defined peaks. Plots of $\partial\log|i_p|/\partial\log|\nu|$ were non-linear due to the transition between different mechanisms.

At the slower sweep rates, an additional pair of peaks (O2, R3) was observed at about +1.27 V vs RHE (+3.53 V vs Li/Li$^+$), which corresponds relatively well to the higher-potential process reported in organic media,[32] and which was also observable in less alkaline LiOH + Li_2SO_4 solutions (Fig. S7). It was observable in the mixed electrolyte, but not the 5.0 M LiOH solution on account of the differing [Li$^+$], which shifted the potential on the RHE scale, moving it into the potential window covered here.

Open circuit behavior.— Another point noted during the comparison of the electrochemical behavior in these electrolytes was the differences in time dependence of the initial open circuit potential (OCP; Fig. S8). While its value was relatively stable over 6 hours in KOH solution, it declined with time in LiOH solution. In the mixed LiOH/KOH solution the OCP increased with time, with the rate of increase being more rapid at higher [Li$^+$] in as-prepared electrolyte. Further investigation would be required to draw definitive conclusions about what process(es) give rise to these trends. Possible contributing factors could include exchange of Li$^+$ with protons on the MnO_2 surface or with Ruetschi[36] or Coleman protons (those associated with Mn^{3+} in the as synthesized material), and phase changes associated with this exchange.

Capacity retention with cycling.— The effect of electrolyte composition and lower potential limit on the capacity retention of γ-MnO_2 during galvanostatic cycling was evaluated for the three compositions considered in the previous section (Fig. 5). Also included in this figure are plots of the fraction of oxidation charge passed during the constant potential step in each cycle. This value is a rough measure of the facility with which the electrode is oxidized; material which is more difficult to oxidize, either because of slow kinetics or low electronic conductivity, will reach the upper potential limit/constant potential step sooner and have a higher value of this ratio.

With a lower potential limit of +0.4 V, the first discharge capacity of γ-MnO_2 in KOH was ~295 mAh/g. A minimum in the differential capacity profile at +0.65 V (Fig. 4a), corresponding to a point at about ~240 mAh/g in the discharge profile, provides a rough measure of the "first-electron" capacity. In comparison, theoretical capacity on a one electron basis is 308 mAh/g. A capacity below the theoretical value (with respect to the one-electron value) can be attributed to combined presence of cation vacancies and Mn^{3+} in the starting material, or to poor utilization.

Electrodes cycled with a +0.6 V cutoff in KOH initially had a lower reduction capacity, which faded more slowly with cycling. Still, by around the 15th cycle, the cells with the higher and lower cutoffs appear to have converged on the same trend (Fig. 5a). The more rapid loss of capacity with discharge to a more negative potential was likely due in large part to the process forming $Mn(OH)_2$, which is converted to birnessite (δ-MnO_2) upon reoxidation, which is then reduced to inactive hausmannite on the subsequent cycle.[37] Additionally this process proceeds via dissolved Mn^{3+} intermediates,[6] which can diffuse away from the working electrode in the flooded cell configuration used here, also contributing to capacity loss.

In LiOH solution, discharge capacity (relative to first cycle capacity) decreased more rapidly while cycling with a higher potential cutoff (+0.6 V) than a lower one. The ratios plotted in Fig. 5b are also suggestive of less facile oxidation in the electrodes discharged to the more positive potential cutoff. This observation is surprising, as generally, reduction to a greater depth of discharge would be expected to be more deleterious to the electrode, particularly for the case of proton insertion into γ-MnO_2.[4,5] However, as a practical matter, a combination of shallow discharge and pure LiOH solutions do not help improve capacity retention, presumably due to the irreversible processes (discussed below) operating in LiOH.

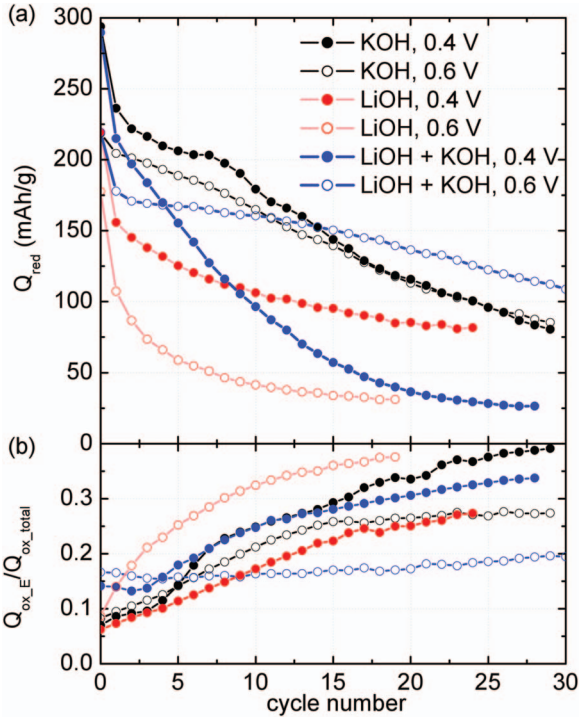

Figure 5. (a) Reduction capacity vs. cycle number for galvanostatic cycling of γ-MnO_2 in several electrolytes at 20 mA/g, with +0.6 V and +0.4 V vs RHE lower potential limits (indicated in legend). In all cases the upper potential limit was +1.35 V vs RHE. The potential was held at +1.35 V vs RHE at the end of galvanostatic oxidation until current had decayed to 2 mA/g or until 10 h had passed. (b) The fraction of the total oxidation charge passed in the constant potential step (Q_{ox_E}/Q_{ox_total}). The electrolyte concentrations were 5.0 M KOH, 5.0 M LiOH, and 0.05 M LiOH + 4.95 M KOH.

Interestingly, by the 15th cycle, the electrode cycled in LiOH/KOH electrolyte to a +0.6 V cutoff had the best capacity and best capacity retention of all of the conditions tested in this work. Also noteworthy is that the fraction of charge passed in the constant potential step changed little over the 25 cycles shown here, indicating little change in the difficulty of oxidizing the electrode under these conditions. When the electrode was discharged to +0.4 V in the mixed solution, however, capacity retention was noticeably worse.

Comparison with R-MnO_2.— Ramsdellite-like MnO_2 (R-MnO_2) was characterized as a point of comparison for γ-MnO_2 (Fig. 6). The two materials showed similar electrochemical behavior, in terms of number and position of voltammetric features. Reduction process R1 in the initial negative-going sweep was also an irreversible process for the case of R-MnO_2 in LiOH, and had almost the same integrated charge as was observed for γ-MnO_2 (84 mAh/g for R-MnO_2 and 92 mAh/g for γ-MnO_2). This small difference indicates that the process is only weakly affected by pyrolusite content and degree of microtwinning, since the diffraction data indicate these values are quite different for the two materials. Incidentally, in KOH solutions, the behavior of R-MnO_2 is *not* similarly analogous to that of γ-MnO_2 (Fig. S9). The charge associated with process R3 was also similar between the two materials, suggesting this process also has a weak dependence on disorder.

The integrated charge of the second reduction process R2 for R-MnO_2 (90 mAh/g) was significantly larger than that for γ-MnO_2

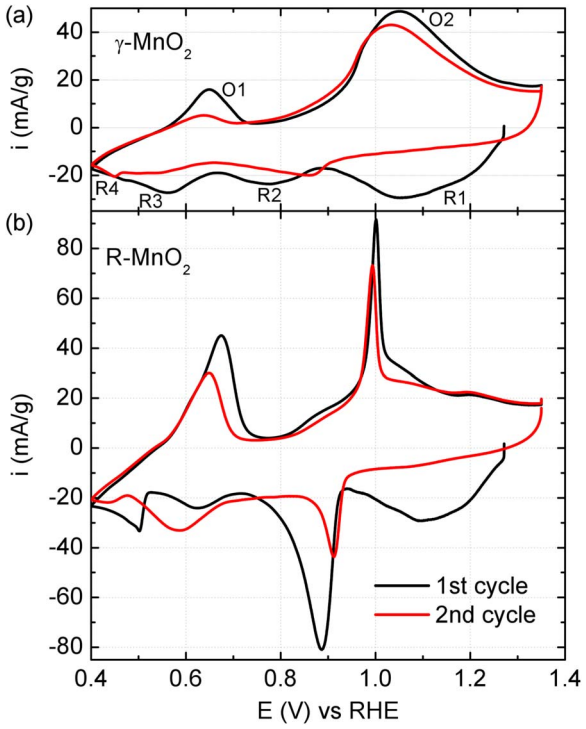

Figure 6. Cyclic voltammograms of γ-MnO_2 and ramsdellite-MnO_2 in 5.0 M LiOH solution at 25 μV/s in 5.0 M LiOH. First cycle in black, second cycle in red.

(55 mAh/g) (Fig. 6). Given the ramsdellite-rich structure of our R-MnO_2 sample as verified by its relatively low measured P_r value (Table I), this second process may correspond to Li-ion uptake by ramsdellite domains. Alternatively, it could be associated with a lesser degree of microtwinning in R-MnO_2, which Jouanneau observed to be correlated with capacity for Li-ion uptake in organic media.[15]

The charge associated with the process forming $Mn(OH)_2$ and its subsequent oxidation (R4 and O1) was greater for R-MnO_2 than for γ-MnO_2 in LiOH solution. Since this reaction is thought to proceed through a dissolution-precipitation path, the greater charge might be due to the distinct, high-aspect ratio morphology of the R-MnO_2 we prepared (Figs. S3,S4); surface area dependence of this process has been already noted for γ-MnO_2 in KOH.[38] When R-MnO_2 was cycled in KOH solution, it was almost entirely converted to $Mn(OH)_2$ in the first cycle, and in the second negative-going sweep, the main feature in the voltammetric profile was a peak associated with birnessite reduction (Fig. S9).

In situ diffraction measurements.— When the γ-MnO_2 underwent reduction in LiOH solution its diffraction peaks shifted to smaller Q values, indicating an increase in d-spacing (Figs. 7a and 8, S9). The initial reduction process R1 involved the continuous deformation of a single phase (i.e. via a solid solution pathway). During this process, some peaks, most conspicuously the $(102)_h$ peak initially at 38.5 nm^{-1}, first broadened significantly and then became sharper again, as would be expected from strain within particles and/or a non-uniform state-of-charge across the electrode at intermediate extent of reduction (Fig. S10a). This degree of width variation was not observed for the $(102)_h$ peak during reduction of γ-MnO_2 in KOH solution (Fig. S10b, S14), indicating a difference in the reaction pathway between reduction in KOH and LiOH solutions.

As noted above, the less defective R-MnO_2 is closely related to γ-MnO_2, differing primarily in long range order. For example, the feature in the R-MnO_2 diffraction pattern analogous to the $(102)_h$ peak is a doublet consisting of the (212) and (402) reflections. This doublet first decreased in intensity and finally disappeared while a

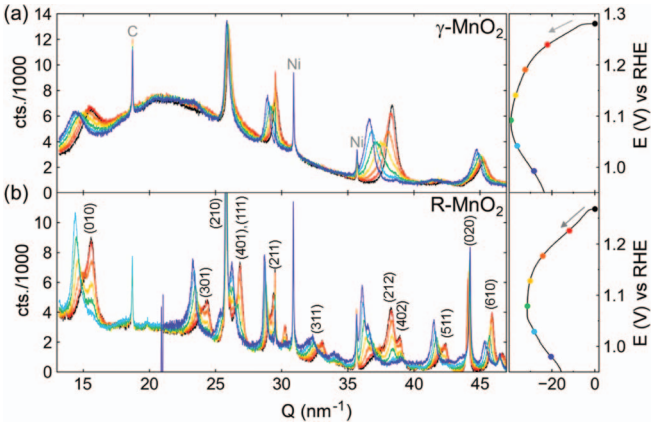

Figure 7. Diffraction patterns of (a) γ-MnO_2 and (b) ramsdellite-MnO_2 measured during the first reduction in 5.0 M LiOH at 25 μV/s, starting from the open circuit potential. Each diffraction pattern was collected over an 11 minute duration (a 16 mV range), though for clarity only every third pattern is shown. At right, the midpoints of the potential ranges over which the patterns were collected are indicated with dots on the voltammetric profile. Peaks associated with graphite and nickel current collector are labeled C and Ni, respectively. The labeled indices for R-MnO_2 refer to the original structure. λ = 0.780138 Å.

new doublet grew in at lower Q. Similar behavior was also evident for the (101), (301), (211) and other less intense peaks. In contrast to the case for γ-MnO_2, for each of these peaks a near-isosbestic point is apparent between the peaks corresponding to the new and old phase (these were not true isosbestic points because the peaks of the new material shifted after it was formed). This suggests the first reduction process we observed in R-MnO_2, proceeds via a two-phase mechanism. The original and new phases must be structurally related given the similarity of their diffraction patterns. While it was being produced, the new phase deformed continuously, indicating a solid solution pathway was also operative simultaneously with the phase transformation. The original phase also showed a small deformation while it was being consumed. The observed breadth of the voltammetric profile of the first reduction process R1 may be due to overlap of the phase transformation and subsequent homogeneous reduction.

Overall, the close correspondence between the patterns for γ-MnO_2 and R-MnO_2 was still present after the first reduction, despite the different pathways (continuous vs. two-phase) that the two materials apparently follow. The observation of a continuous deformation for γ-MnO_2 and a well-defined phase transformation for R-MnO_2 is

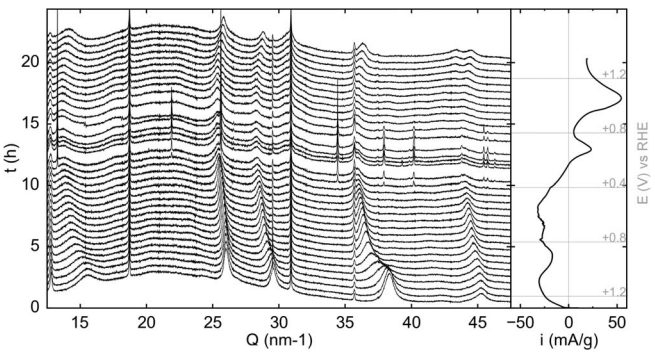

Figure 8. Diffraction patterns of an γ-MnO_2 electrode measured during one potential cycle in 5.0 M LiOH, with current shown at the right. Each pattern was collected over an 11 minute interval, but for clarity, only every third pattern is shown. The set of narrow peaks arising near the lower potential limit correspond to $Mn(OH)_2$. Potential sweep rate: 25 μV/s; λ = 0.780138 Å.

Table II. Lattice parameters of R-MnO_2 at selected potentials during first negative-going potential sweep, and percent change over the potential intervals.

	E (V) vs RHE		
Parameter (Å)	1.28 V (open circuit)	0.92 V	0.56 V
a	9.40	9.61	10.17
b	2.84	2.83	2.79
c	4.44	4.99	5.00
	Potential range		
% change	1.28 V to 0.92 V	0.92 V to 0.56 V	1.28 V to 0.56 V
a	2.3	5.8	8.2
b	−0.44	−1.6	−2.1
c	12.4	0.20	12.6

possibly related to the relative rate capabilities of these two materials, e.g. due the high aspect ratio morphology of the R-MnO_2 particles. It has been noted that the structural evolution of γ-MnO_2 can be affected by rate of reduction for Li-ion insertion in organic media.[39] At low rates in organic Li-ion containing media, the reduction was reported to proceed via a two phase mechanism, while at high rates, the structure deformed in a continuous manner as a solid solution. The observed non-monotonic variation of the width of the $(102)_h$ peak with reduction of γ-MnO_2 (Fig. S10a) may relate to the development of strain during a homogenous transformation in structures midway between original and new phases.

The R-MnO_2 lattice deformation was highly anisotropic during reduction (Table II, Fig. S11). In particular, *c* direction (Fig. 1) of R-MnO_2 underwent a large expansion during the first reduction R1. As the potential was swept through reduction processes R2 and R3, the *a* lattice parameter then expanded while there was little further change in the *c* dimension. The *b* direction underwent relatively small contraction. For the deformation of the structure to occur primarily in the *ac* plane (i.e. the plane orthogonal to the 2 × 1 tunnels of ramsdellite) is consistent with what has been reported both for proton[10,21,40,41] and lithium ion insertion.[23]

Comparison of our R-MnO_2 data set with published diffraction patterns for R-MnO_2 chemically reduced in lithium-ion containing organic media[23] suggests that the structural evolution of the material is similar under the two sets of reduction conditions (Fig. S12). In the reported work,[23] an initial two-phase mechanism was not observed, but that may be because the transformation was already completed for the first sample had already been reduced to $Li_{0.3}MnO_2$. The present data indicate that the first reduction process was complete or near complete at that degree of reduction.

The ex situ diffraction pattern of a γ-MnO_2 electrode which had undergone several slow potential cycles in LiOH electrolyte differed significantly from that at the end of the first cycle observed in situ, indicating that the structure continues to evolve with cycling (Fig. 9). The pattern of the cycled material resembled that of $LiMn_2O_4$ spinel, though the relative intensities of the peaks were different and some peaks were missing. While Mn_3O_4 and $ZnMn_2O_4$ are also spinel phases, their diffraction patterns do not appear to match quite as well as that of $LiMn_2O_4$ (Fig. S13). The pattern of the cycled material matches particularly well with that reported for the product of LT-$LiMnO_2$ electrooxidation in organic media, which was similar to the patterns of $Li[Li_xMn_{2-x}]O_4$ defect spinels.[42] The designation 'LT' indicated synthesis in the 300–450°C range. Reimers et al. also found LT-$LiMnO_2$ to be oxidized to a disordered spinel phase.[43] It has been noted that other manganese oxides, including pyrolusite MnO_2, $Li_{0.33}MnO_2$ (synthesized by heating γ-MnO_2 with lithium nitrate), and layered $LiMnO_2$ can be converted to a spinel phase during reduction or cycling.[44,45,46] Spinel phase lithium manganese oxides are expected to show capacity in this potential range, but with rapid degradation.[47]

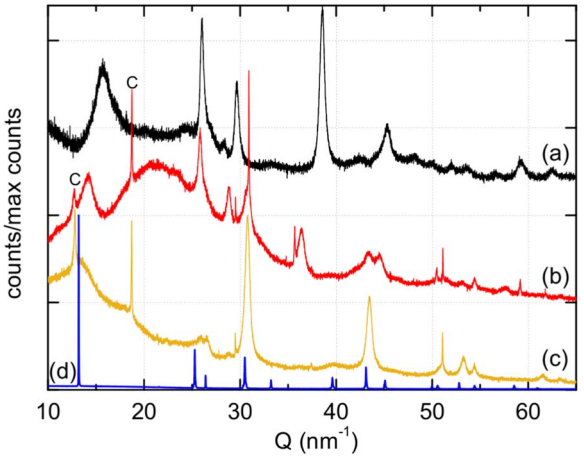

Figure 9. Diffraction patterns of (a) γ-MnO_2 powder, (b) γ-MnO_2 after one cycle in LiOH solution in situ, (c) γ-MnO_2 after several cycles in LiOH solution ex situ, (d) $LiMn_2O_4$ powder. λ = 0.780138 Å.

Conclusions

Differences between the electrochemical behavior of γ-MnO_2 in KOH and LiOH solutions were characterized. In the former case, protons are the intercalating species, while in the latter case, both lithium ions and protons appear to intercalate in competition, with lithium intercalation favored at higher $[Li^+]$ and at lower rates. Use of LiOH in place of KOH did not improve the capacity or capacity retention of γ-MnO_2 during galvanostatic cycling. There are some indications that processes such as $Mn(OH)_2$ formation are diminished in LiOH due to solubility effects; however, solid-state irreversible transformations driven by Li^+ appear to negate any improvements capacity retention which might be expected from such effects. Due to the irreversible process, shallow discharge cycling protocols will not improve capacity retention with cycling, as has been reported for γ-MnO_2 in KOH solutions. While γ-MnO_2 is reported to undergo gradual transformation to inactive Mn_3O_4 and $ZnMn_2O_4$ phases in KOH solutions, the inactive phase formed during long term cycling in LiOH appeared to be a different spinel-like product. Use of a mixed LiOH/KOH solution improved the cyclability of the γ-MnO_2 over that in either pure LiOH or KOH. The lower concentration of Li^+ present in the mixed LiOH/KOH solution may have slowed the rate of formation of the inactive, spinel-like phase in comparison to concentrated LiOH solution, while at the same time allowing for selective Li^+ uptake at surface/defect sites.

The irreversible structural changes γ-MnO_2 underwent during reduction in LiOH solution appear to be analogous to those we observed in R-MnO_2. In the latter case, the structure of the reduced material appears to be similar to that reported for chemical reduction of R-MnO_2 in organic media. Under the conditions we used for in situ diffraction experiments, the irreversible first reduction process followed a solid-solution reaction in γ-MnO_2 and a sequence of soli-solution/two-phase/solid-solution reactions in R-MnO_2.

Acknowledgments

This work was supported by the Laboratory Directed Research and Development program of Brookhaven National Laboratory (LDRD-BNL) under Contract No. DE-AC02-98CH 10866 with the U.S. Department of Energy. Use of the National Synchrotron Light Source, Brookhaven National Laboratory, was supported by the U.S. Department of Energy, Office of Science, Office of Basic Energy Sciences, under Contract No. DE-AC02-98CH10886. This research used resources of the Center for Functional Nanomaterials, which is a U.S. DOE Office of Science Facility, at Brookhaven National Laboratory under Contract No. DE-SC0012704. We thank Dr. Jianqing Zhao for assistance with the Rigaku diffractometer.

References

1. J. W. Gallaway, M. Menard, B. Hertzberg, Z. Zhong, M. Croft, L. A. Sviridov, D. E. Turney, S. Banerjee, D. A. Steingart, and C. K. Erdonmez, *Journal of the Electrochemical Society*, **162**, A162 (2015).
2. A. Kozawa and R. A. Powers, *Journal of the Electrochemical Society*, **113**, 870 (1966).
3. T. Ohzuku, H. Tomura, and K. Sawai, *Journal of the Electrochemical Society*, **144**, 3496 (1997).
4. N. D. Ingale, J. W. Gallaway, M. Nyce, A. Couzis, and S. Banerjee, *Journal of Power Sources*, **276**, 7 (2015).
5. K. Kordesch, J. Gsellmann, M. Peri, K. Tomantschger, and R. Chemelli, *Electrochimica Acta*, **26**, 1495 (1981).
6. D. Im, A. Manthiram, and B. Coffey, *Journal of the Electrochemical Society*, **150**, A1651 (2003).
7. M. R. Bailey and S. W. Donne, *Journal of the Electrochemical Society*, **159**, A2010 (2012).
8. M. Minakshi, P. Singh, D. R. G. Mitchell, T. B. Issa, and K. Prince, *Electrochimica Acta*, **52**, 7007 (2007).
9. P. M. De Wolff, *Acta Crystallographica*, **12**, 341 (1959).
10. Y. Chabre and J. Pannetier, *Progress in Solid State Chemistry*, **23**, 1 (1995).
11. R. X. Fischer, *J. Appl. Cryst*, **18**, 258 (1985).
12. P. Ruetschi and R. Giovanoli, *Journal of the Electrochemical Society*, **135**, 2663 (1988).
13. A. P. Malloy, G. J. Browning, and S. W. Donne, *Journal of Colloid and Interface Science*, **285**, 653 (2005).
14. W. I. Jung, K. Sakamoto, C. d. Pitteloud, N. Sonoyama, A. Yamada, and R. Kanno, *Journal of Power Sources*, **174**, 1137 (2007).
15. S. Jouanneau, S. Sarciaux, A. Le Gal La Salle, and D. Guyomard, *Solid State Ionics*, **140**, 223 (2001).
16. M. Minakshi, P. Singh, M. Carter, and K. Prince, *Electrochemical and Solid State Letters*, **11**, A145 (2008).
17. M. E. Taboada, D. M. Véliz, H. R. Galleguillos, and T. A. Graber, *J. Chem. Eng. Data*, **50**, 187 (2005).
18. L. G. Hepler and G. Olofsson, *Chemical Reviews*, **75**, 585 (1975).
19. M. Pourbaix, *Atlas of Electrochemical Equilibria in Aqueous Solutions*, National Association of Corrosion Engineers: Houston, Texas, 1974.
20. E. L. Littauer and K. C. Tsai, *Journal of the Electrochemical Society*, **123**, 771 (1976).
21. J. E. Post and P. J. Heaney, *American Minerologist*, **89**, 969 (2004).
22. M. H. Rossouw, A. de Kock, D. C. Liles, R. J. Gummow, and M. M. Thackeray, *Journal of Materials Chemistry*, **2**, 1211 (1992).
23. M. M. Thackeray, M. H. Rossouw, R. J. Gummow, D. C. Liles, K. Pearce, A. De Kock, W. I. F. David, and S. Hull, *Electrochimica Acta*, **38**, 1259 (1993).
24. D. Larcher, P. Courjal, R. Herrera Urbina, B. Gérand, A. Blyr, A. du Pasquier, and J.-M. Tarascon, *Journal of the Electrochemical Society*, **145**, 3392 (1998).
25. D. Balachandran, D. Morgan, and G. Ceder, *Journal of Solid State Chemistry*, **166**, 91 (2002).
26. Y. Paik, W. Bowden, T. Richards, R. Sirotina, and C. P. Grey, *Journal of the Electrochemical Society*, **151**, A998 (2004).
27. Y. P. Chabre, *Journal of the Electrochemical Society*, **138**, 329 (1991).
28. S. W. Donne, G. A. Lawrance, and D. A. J. Swinkels, *Journal of the Electrochemical Society*, **144**, 2961 (1997).
29. R. Patrice, B. Gérand, J. B. Leriche, L. Seguin, E. Wang, R. Moses, K. Brandt, and J. M. Tarascon, *Journal of the Electrochemical Society*, **148**, A448 (2001).
30. H. Kim, J. Hong, K.-Y. Park, H. Kim, S.-W. Kim, and K. Kang, *Chemical Reviews*, **114**, 11788 (2014).
31. J. C. Nardi, *Journal of the Electrochemical Society*, **132**, 1787 (1985).
32. W. I. Jung, M. Nagao, C. Pitteloud, K. Itoh, A. Yamada, and R. Kanno, *Journal of Materials Chemistry*, **19**, 800 (2009).
33. D. A. Lown and H. R. Thirsk, *Transactions of the Faraday Society*, **67**, 132 (1971).
34. M. Minakshi and P. Singh, *Journal of Solid State Electrochemistry*, **16**, 1487 (2012).
35. Q. Shu, L. Chen, Y. Xia, X. Gong, and X. Gu, *The Journal of Physical Chemistry C*, **117**, 6929 (2013).
36. W. Bowden, C. P. Grey, S. Hackney, F. Wang, Y. Paik, N. Iltchev, and R. Sirotina, *Journal of Power Sources*, **153**, 265 (2006).
37. J. McBreen, *Electrochimica Acta*, **20**, 221 (1975).
38. S. W. Donne, G. A. Lawrance, and D. A. J. Swinkels, *Journal of the Electrochemical Society*, **144**, 2954 (1997).
39. W. M. Dose, N. Sharma, and S. W. Donne, *Journal of Power Sources*, **258**, 155 (2014).
40. L. A. H. MacLean and F. L. Tye, *J. Mater. Chem.*, **7**, 1029 (1997).
41. L. A. H. MacLean and F. L. Tye, *Journal OF Solid State Chemistry*, **123**, 150 (1996).
42. T. Ohzuku, S. Kitano, M. Iwanaga, H. Matsuno, and A. Ueda, *Journal of Power Sources*, **68**, 646 (1997).
43. J. N. Reimers, E. W. Fuller, E. Rossen, and J. R. Dahn, *Journal of the Electrochemical Society*, **140**, 3396 (1993).
44. W. I. F. David, M. M. Thackeray, P. G. Bruce, and J. B. Goodenough, *Materials Research Bulletin*, **19**, 99 (1984).
45. E. Levi, E. Zinigrad, H. Teller, M. D. Levi, D. Aurbach, E. Mengeritsky, E. Elster, P. Dan, E. Granot, and H. Yamin, *Journal of the Electrochemical Society*, **144**, 4133 (1997).
46. A. R. Armstrong, N. Dupre, A. J. Paterson, C. P. Grey, and P. G. Bruce, *Chemistry of Materials*, **16**, 3106 (2004).
47. R. J. Gummow and M. M. Thackeray, *Journal of the Electrochemical Society*, **141**, 1178 (1994).